ChemComm

COMMUNICATION

View Article Online
View Journal | View Issue

Cite this: *Chem. Commun.*, 2023, 59, 2323

Received 3rd October 2022,
Accepted 27th January 2023

DOI: 10.1039/d2cc05413b

rsc.li/chemcomm

High Seebeck coefficient thermogalvanic cells *via* the solvent-sensitive charge additivity of cobalt 1,8-diaminosarcophagine†

Kristine Laws, [a] Mark A. Buckingham, ‡[a] Matthew Farleigh,[b] Michelle Ma [b] and Leigh Aldous *[a]

Thermogalvanic devices can chemically convert low grade (<200 °C) waste thermal energy into electrical energy. A temperature gradient across the device drives an entropically favourable electrochemical redox reaction, resulting in continuous current production. The voltage correlates with the entropy change during the redox reaction, which favours high valence metal complexes with high charge densities. Here we investigate cobalt (II/III) sarcophagine ([Co(SAR)]$^{2+/3+}$) for application in thermogalvanic cells, as a function of solvent; the two uncoordinated amine groups 1,8-diaminosarcophagine are typically protonated to form tetra-cationic/pentacationic [Co(SARH$_2$)]$^{4+/5+}$. In water, [Co(SARH$_2$)]$^{4+/5+}$ gave a thermogalvanic Seebeck coefficient (S_e) of +0.43 mV K^{-1}, which is entropically consistent with just the Co$^{2+/3+}$ core valence, whereas DMSO and ionic liquid solvents gave S_e values of +1.84 and +2.04 mV K^{-1}, respectively, in line with the 'Co$^{4+/5+}$' overall complex. This work proves how the ionic charge on pendant moieties can undergo charge-additivity with the metal core to significantly boost entropically-driven processes, but only in suitably low dielectric and bulky solvents.

Thermogalvanic cells (or thermocells) can convert thermal to electrical energy using an entropically driven redox process.[1,2] These electrolyte-based systems rely upon an oxidised and reduced species to act as charge carriers between a hotter electrode and a colder electrode, analogous to the classic Seebeck effect demonstrated by many solid conductors and semi-conductors when exposed to a temperature gradient.[1,2] When a temperature difference (ΔT) induces a voltage (ΔV), this is typically reported as a ratio of the two as the Seebeck coefficient (S_e, V K^{-1}), as shown by:

$$S_e = \frac{\Delta T}{\Delta V} = \frac{\Delta S_{rc}}{nF} \quad (1)$$

In thermocells, this thermogalvanic S_e strongly correlates with the entropy difference between the two redox states, ΔS_{rc}, divided by the number of electrons transferred, n, and the Faraday constant, F. The S_e dictates both the voltage of the electrical power produced by the cell, and drives the current production in line with Butler–Volmer kinetics.[3] High valence redox couples such as Fe$^{2+/3+}$,[4–6] [Fe(CN)$_6$]$^{3-/4-}$,[3,7,8] and [Co(bpy)$_3$]$^{2+/3+}$,[9–11] typically result in good S_e values. This also correlates with the overall efficiency of the thermocell at generating electricity, and therefore device viability.[12]

Other methods have been reported to boost S_e *via* entropy-boosting effects, such as thermosensitive crystallisation[13] and host–guest complexation.[14] The typically minor Soret effect contributions[1] to S_e have also been boosted in certain systems, to significantly increase the overall S_e.[15] However, the former systems are orientation and gravity sensitive, while the latter S_e increase did not correspond to boosted current production. Achieving higher S_e *via* highly charged but fully soluble redox couples will result in improved devices with minimal complexity; there are limited reports of this being achieved *via* spin-crossover in complexes[16] (such as [Co(bpy)$_3$]$^{2+/3+}$),[9] and the solvent shell *via* additives.[8] This report explores a third method, utilising charge additivity. This covers the barely explored concept of tethering a non-redox active charge adjacent to a redox-active moiety, to achieve a higher S_e.[19] This has only previously been demonstrated in an ionic liquid and using a ferrocene species.[19]

Sarcophagines are caged ligands capable of forming very stable metal–ligand complexes,[20] with extensive medical[21,22] and catalytic[23] applications. The cobalt-based 1,8-diamino-sarcophagine complex has two free amine groups which, under acidic conditions, are protonated to afford a 5+ Co(III) complex ([Co^{III}(SARH$_2$)]$^{5+}$).[20] Because it has a formal Co$^{2+/3+}$ redox centre

[a] *Department of Chemistry, King's College London, London, SE1 1DB, UK. E-mail: leigh.aldous@kcl.ac.uk*
[b] *School of Biomedical Engineering and Imaging Sciences, King's College London, St. Thomas' Hospital, London, SE1 7EH, UK*

† Electronic supplementary information (ESI) available: Detailed synthetic and experimental details; solvent and pH effect upon CVs; tabulated thermogalvanic data. See DOI: https://doi.org/10.1039/d2cc05413b

‡ Current address: Department of Materials, University of Manchester, Sackville Street, Manchester, M13 9PL, UK.

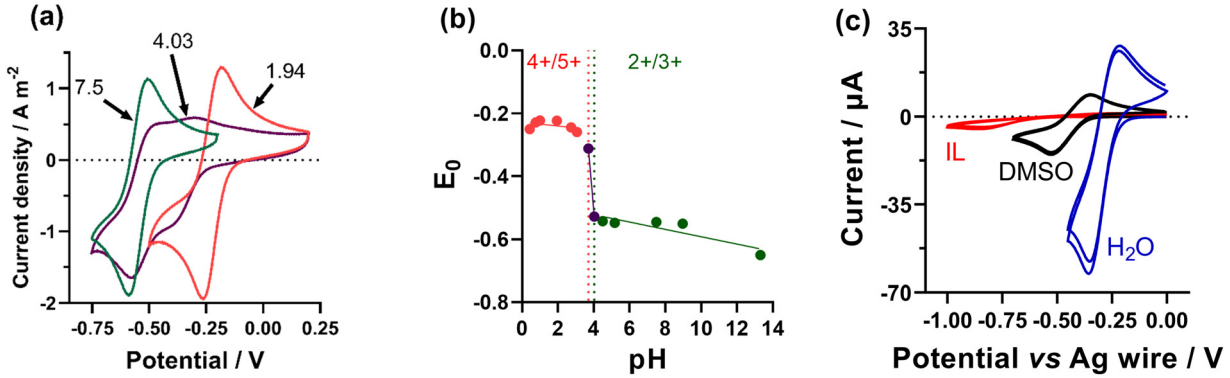

Fig. 1 (a) Cyclic voltammetry of aqueous $[Co(SAR)](OTf)_5$ solutions at different pH; 0.1 M HCl (1.94, red line), HCl/NaOH (4.03, purple line) and 0.1 M NaOH (7.5, green line). (b) Graph showing pH titration, E^0 *vs.* pH, of $[Co(SAR)][OTf]_5$ in aqueous environments, from 0.1 M HCl to 1.0 M NaOH, demonstrating transition from $[Co(SAR)][OTf]_5$ (acidic, red dots), $[Co(SAR)][OTf]_3$ (basic, green dots), and mix of the protonated/deprotonated [Co(SAR)] (pH ~4, purple dots). (c) CVs of 5 mM $[Co(SAR)][OTf]_5$ recorded in aqueous, DMSO and ionic liquid electrolytes (see ESI† for full details and individual scans, both neat and acidified). All recorded under Ar, at an Au working electrode.

but an overall delocalised complex charge of $[Co(SARH_2)]^{4+/5+}$, it was studied in a thermogalvanic cell to explore the possibilities and limitations of charge additivity in metal complexes.

First, it was necessary to ensure the 5+ complex was dominant in solution, and redox chemistry could be observed. Therefore the complex $[Co(SARH_2)][OTf]_5$ was synthesised, and full details can be found in the ESI.† The electrochemical properties of $[Co^{III}(SARH_2)]^{5+}$ were first investigated, to ensure full protonation was achieved. When dissolved in 0.1 M HCl (10 mM $[Co(SARH_2)][OTf]_5$, pH 1.94) a single reversible redox couple was observed for the reduction from Co^{III} to Co^{II}, as shown by the red line in Fig. 1(a). A wide spectrum of pH values were then explored by combining 0.1 M HCl and 0.1 M NaOH in different ratios; two distinct reversible redox couples were observed at pH < 3 and pH > 4, while around pH 4 both redox couples were present (as shown by the CVs in Fig. 1(a)). Plotting the obtained E^0 values of the predominant redox couple *vs.* pH (Fig. 1(b)) highlights the transition clearly, which corresponds well to the reported $pK_{a,1}$ and $pK_{a,2}$ values of *ca.* 3.3.[20] Therefore in 0.1 M HCl, the $Co^{II/III}$ redox process is present, stable, and corresponds to the $[Co^{III}(SARH_2)]^{5+}$ species in solution.

The same $[Co(SARH_2)][OTf]_5$ species was also investigated in DMSO and $[Emim][NTf_2]$, except 0.1 M HCl was substituted for 0.1 M anhydrous triflic acid (HOTf). Reversible $Co^{II/III}$ redox couples were also observed in these electrolytes (Fig. 1(c), and Fig. S1; see ESI† for full details).

Next, their thermogalvanic properties were investigated. The measured S_e correlates directly to the ΔS_{rc}, and the ΔS_{rc} broadly corresponds to the charge density of the redox couple and the degree of solvent interaction; Hupp and Weaver demonstrated that for a wide range of low-spin metal complexes, it can approximated by the following equation:[16]

$$\Delta S_{rc} = 91.5 - 2.43AN + 86.6\frac{(Z_{ox}^2 - Z_{red}^2)}{r} \qquad (2)$$

where AN is the solvent acceptor number, Z_{ox} and Z_{red} are the charge on the oxidised and reduced species, respectively, and r is the ionic radius (Å).[16] This is only an empirical relationship but captures the majority of solute–solvent interactions which, if different, result in an entropy change. Its temperature dependence (if any) has not been extensively explored, but it has been successfully used to correlate thermogalvanic measurements with solution-phase dynamics of metal complexes.[17,18] While the charge valence is clearly an influential parameter, it has conventionally been limited to cationic metal$^{2+/3+}$ ($Z_{ox}^2 - Z_{red}^2 = 5$) or anionic [complex]$^{3-/4-}$ ($Z_{ox}^2 - Z_{red}^2 = 7$) systems, due to lack of readily available and stable systems outside of this spectrum of charges.

Before measuring the thermogalvanic properties, this required synthesising the air-sensitive $[Co^{II}(SARH_2)]^{4+}$, as well as increasing the concentration from 10 mM to 50 mM to get stable power measurements. Full details are included in the ESI,† but briefly for the aqueous system two 50 mM solutions of $[Co^{III}(SARH_2)][OTf]_5$ were prepared in 0.1 M HCl. One solution was reduced to the Co^{II} by stirring with amalgamated zinc nuggets for 30 minutes, then decanting from the zinc; the two solutions were then mixed in a 50 : 50 ratio to yield a solution containing 0.1 M HCl, 25 mM $[Co^{II}(SARH_2)]^{4+}$ and 25 mM $[Co^{III}(SARH_2)]^{5+}$ (pH 1.33). This solution was injected into a previously reported thermogalvanic cell[24] for measurement, with all handling performed under an argon atmosphere.

The Seebeck coefficient of this aqueous $[Co(SARH_2)]^{4+/5+}$ solution was measured in triplicate, and was found to be +0.43 ± 0.02 mV K^{-1}. Using eqn (2), the average radius of this sarcophagine species, and the acceptor number of water, it's possible to calculate the expected S_e for two scenarios; either the solvating water molecules experience the full valence of the complex (*i.e.* Z_{ox} = +5, Z_{red} = +4) or only experiences the valence charge of the $Co^{II/III}$ metal centre and solvation around the pendant $-NH_3^+$ moieties remain unaltered during the redox process (*i.e.* Z_{ox} = +3, Z_{red} = +2). The predicted S_e values are +1.18 mV K^{-1} and +0.47 mV K^{-1} for the $[Co(SARH_2)]^{4+/5+}$ and $Co^{2+/3+}$ ($SARH_2^{2+}$) cases, respectively. Clearly the experimentally measured value of +0.43 ± 0.02 mV K^{-1} corresponds to the entropy difference between a 2+ and 3+ valence complex (with the smaller experimental value in line with the electrolyte's high ionic strength[3]), and therefore additivity of charge for $[Co(SARH_2)]^{4+/5+}$ cannot be observed in the aqueous media.

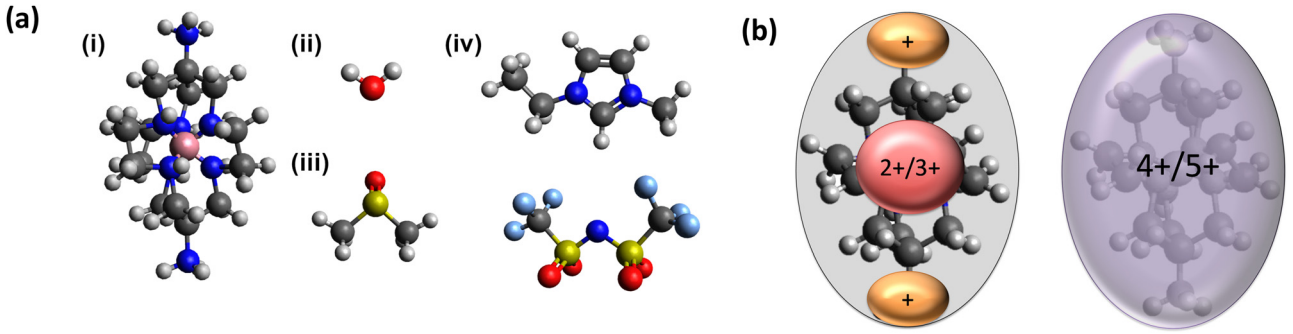

Fig. 2 Structural representations comparing (a) the size of (i) [Co(SARH$_2$)] to solvent molecules (ii) water, (iii) DMSO and (iv) ionic liquid (1-ethyl-3-methylimidazolium bis(trifluoromethylsulfonyl)imide, [Emim][NTf$_2$]), and (b) highlighting the possible division of charge in the [Co(SARH$_2$)] complex, with the central Co valence being solvated separately to the amino charges by smaller solvent molecules (*cf.* water), or demonstrate charge-additivity across the complex by larger solvating species which cannot discriminate between the Co valence charge and the fixed amino charges.

This lack of additivity of charge can be attributed to the relative size of the solvent and the solute, which is shown visually in Fig. 2. A water molecule in the inner solvation sphere around the core of the $[Co(SARH_2)]^{4+/5+}$ species is highly unlikely to directly interact with the $-NH_3^+$ pendant groups, and *vice versa*.

In theory, the S_e of $[Co(SARH_2)]^{4+/5+}$ should be largely pH independent, and some experiments were performed to explore this. However, the $[Co^{II}(SARH_2)]^{4+}$ species was found to be very sensitive to pH, with any addition of NaOH resulting in precipitation. Moving to an acetate buffer, similar S_e values were measured under acidic conditions ($+0.48 \pm 0.04$ mV K^{-1}, pH 2.02) but demonstrated a S_e inversion under the highest pH conditions that were stable (-0.77 ± 0.02 mV K^{-1}, pH 6.29), indicating the entropic pathway has been reversed.[18] This surprising observation is discussed in more detail in the ESI† (Fig. S2–S5), but is tentatively attributed to a difference in the pK_a of the two redox states, and solvation of dissociated protons drove the overall value of ΔS_{rc}.

Next, the same experiment was repeated in DMSO; the measured S_e was $+1.84 \pm 0.02$ mV K^{-1}, which is closer to the calculated S_e for the charge-additive $[Co(SARH_2)]^{4+/5+}$ species (+2.08 mV K^{-1}) than for just the $Co^{2+/3+}(SARH_2^{2+})$ scenario (+1.36 mV K^{-1}). All the S_e are also summarised in Table 1, for convenient comparison (all recorded at $\Delta T = 20$ K and $T_c = 20$ °C).

Table 1 Comparison of the observed Seebeck coefficients measured for 50 mM $[Co(SARH_2)]^{4+/5+}$ in the indicated solvent and 0.1 M acid (HCl for H_2O, triflic acid for DMSO and IL), compared against their calculated Seebeck coefficients for the $Co^{2+/3+}(SARH_2^{2+})$ and $[Co(SARH_2)]^{4+/5+}$ hypothetical scenarios (using eqn (2), which assumes dilute solutions with a low ionic strength[16]). All Observed Seebeck values recorded at $\Delta T = 20$ K and $T_c = 20$ °C; temperature dependency was not explored in this preliminary study

Solvent	Observed Seebeck (mV K^{-1})	Calculated Seebeck (mV K^{-1})	
		"$Co^{2+/3+}(SARH_2^{2+})$"	$[Co(SARH_2)]^{4+/5+}$
H_2O	$+0.48 \pm 0.04$	+0.47	+1.18
DMSO	$+1.84 \pm 0.02$	+1.36	+2.08
IL	*ca.* +2.0[a]	+1.16	+1.87

[a] Value is tentative due to suspended material in the IL and potentially not achieving a 50 : 50 ratio of $[Co^{II}(SARH_2)]^{4+}$: $[Co^{III}(SARH_2)]^{5+}$.

Therefore, significant charge additivity is occurring, which is again rationalised by the relative scales in Fig. 2; inner solvation sphere DMSO molecules around the metal centre and $-NH_3^+$ moieties are likely to be directly adjacent, without any screening spectator molecules in-between. The lower dielectric constant of DMSO will also result in a dimensionally larger outer solvation sphere, which will be more susceptible to the overall complex charge.

Finally, the experiment was repeated in the ionic liquid [Emim][NTf$_2$], but this was experimentally more challenging; the zinc reduction proceeded very slowly, resulted in a suspension rather than a clear solution (likely Zn(Hg) particles), and alternative reducing agents were also unsuccessful (full details in ESI†). Measuring the OCP demonstrated overnight reduction achieved significant conversion of Co^{III} to Co^{II}, and using this an S_e value of *ca.* +2.0 mV K^{-1} was measured. This value is again consistent with the charge additive scenario (+1.87 mV K^{-1}) rather than the $Co^{2+/3+}(SARH_2^{2+})$ scenario (+1.16 mV K^{-1}), in line with initial expectations that the extremely bulky ionic liquid ions would experience the combined ionic charge of the complex. However, these measurements were temperamental, and a precise 50 : 50 ratio of Co^{II} to Co^{III} cannot be guaranteed (NB: non-equimolar ratios are known to affect the measured S_e by up to ±15%[3]).

Finally, the effect of this charge additivity was evaluated by comparing the thermogalvanic power generated by 50 mM $[Co(SARH_2)]^{4+/5+}$ in aqueous 0.1 M HCl *vs.* 50 mM $[Co(SARH_2)]^{4+/5+}$ in DMSO containing 0.1 M TfOH (Fig. 3). As shown by the CV comparison (ESI,† Fig. S1) in DMSO the system suffered from slower electron kinetics and *ca.* 4-fold slower mass transport, which should result in significantly lower power generation. Fig. 3 shows the resultant *j*–*V* and power curves; both solvents demonstrated the linear *j*–*V* trend and polynomial power curves expected for a continuous, steady-state thermogalvanic cell.[24]

Overall the DMSO system generated 3-fold more power than the aqueous system. In DMSO the charge additive aspect boosted the S_e 3.8-fold; since a higher S_e boosts both voltage and current, relative thermogalvanic power is approximately related to the S_e squared (excluding kinetic and mass transport aspects).[3,25] Here $3.8^2 = 14.4$, but a 14-fold increase in power was not demonstrated in DMSO, likely due to the much slower

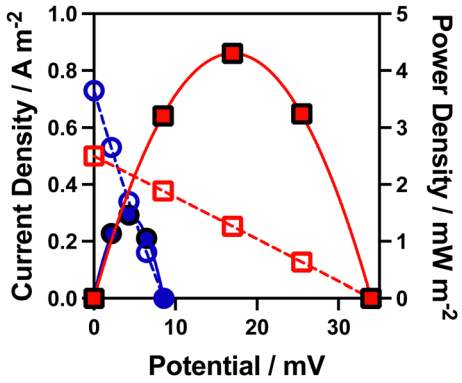

Fig. 3 The current density and power density of [Co(SAR)](OTf)$_{4/5}$ (25 mM each of Co(II/III)) thermocells for (blue circles) aqueous 0.1 M HCl (pH 1.33), and (red squares) DMSO containing 0.1 M HOTf. Hollow symbols and dashed lines correspond to j–V plots, and filled symbols and solid lines to P–V plots. Measured at gold electrodes with ΔT = 20 K and T_c = 20 °C; the figure shows one representative measurement, while the average values from triplicate measurements are tabulated in the ESI.†

kinetics and mass transport in DMSO. So charge-additivity achieved a 3-fold boost primarily due to the higher S_e, with significant scope for further improvement (up to 14-fold) by improved mass transport and electrocatalysis.

Something that was not studied was the genuine efficiency[12] of these thermocells; however, the much lower thermal conductivity of DMSO (0.186 W m^{-1} K^{-1})[26] over water (0.607 W m^{-1} K^{-1})[27] would suggest even higher efficiency in DMSO.[12] Prior studies have investigated mixtures of water, DMSO and [Emim][NTf$_2$] in thermogalvanic cells;[28] the aqueous system displayed an order of magnitude higher diffusion coefficients than in DMSO, although pure DMSO still generated the highest power. Solvent mixtures in this charge-additive system might result in different outcomes.

A prior study tethered a cationic imidiazolium group to a ferrocene/ferrocenium redox couple, and the Seebeck coefficient doubled (to S_e = +0.23 mV K^{-1}) in an ionic liquid.[19] In conclusion to the work reported here, a cobalt sarcophagine cage complex has been used in a thermogalvanic cell for the first time. Protonation of the cage itself was capable of boosting the overall redox-induced entropy change *via* charge-additivity (S_e up to +2.08 mV K^{-1}) and so boost thermogalvanic power production. However, this study has demonstrated that this effect is only observed in non-aqueous media. Going forwards, iron is arguably a more sustainable metal, and spin crossover has been reported in the analogous [Fe$^{II/III}$(SARH$_2$)]$^{4+/5+}$ system;[20] this is expected to boost the S_e even further. It will also be of interest to see how this charge-additive effect can be combined with other S_e-boosting effects such as solvent coordination, crystallisation and host–guest interactions, since each boost in S_e can increase the overall genuine efficiency of these devices at waste heat valorisation.[12]

Conflicts of interest

There are no conflicts to declare. Chemicals and experimental methods can be found in the ESI,† as well as the effect of solvent and pH upon cyclic voltammograms, and tabulated thermogalvanic data.

Notes and references

1 T. I. Quickenden and Y. Mua, *J. Electrochem. Soc.*, 1995, **142**, 3985–3994.
2 M. F. Dupont, D. R. MacFarlane and J. M. Pringle, *Chem. Commun.*, 2017, **53**, 6288–6302.
3 M. A. Buckingham, S. Hammoud, H. Li, C. J. Beale, J. T. Sengel and L. Aldous, *Sustainable Energy Fuels*, 2020, **4**, 3388.
4 M. A. Buckingham, F. Marken and L. Aldous, *Sustainable Energy Fuels*, 2018, **2**, 2717.
5 K. Kim, S. Hwang and H. Lee, *Electrochim. Acta*, 2020, **335**, 135651.
6 J. H. Kim, J. H. Lee, R. R. Palem, M. S. Suh, H. H. Lee and T. J. Kang, *Sci. Rep.*, 2019, **9**, 8706.
7 B. Burrows, *J. Electrochem. Soc.*, 1976, **123**, 154–159.
8 J. Duan, G. Feng, B. Yu, J. Li, M. Chen, P. Yang, J. Feng, K. Liu and J. Zhou, *Nat. Commun.*, 2018, **9**, 1–8.
9 T. J. Abraham, D. R. Macfarlane and J. M. Pringle, *Energy Environ. Sci.*, 2013, **6**, 2639–2645.
10 A. Taheri, D. R. MacFarlane, C. Pozo-Gonzalo and J. M. Pringle, *Electrochim. Acta*, 2019, **297**, 669–675.
11 N. Jiao, T. J. Abraham, D. R. MacFarlane and J. M. Pringle, *J. Electrochem. Soc.*, 2014, **161**, D3061–D3065.
12 M. A. Trosheva, M. A. Buckingham and L. Aldous, *Chem. Sci.*, 2022, **13**, 4984.
13 B. Yu, J. Duan, H. Cong, W. Xie, R. Liu, X. Zhuang, H. Wang, B. Qi, M. Xu, Z. L. Wang and J. Zhou, *Science*, 2020, **370**, 342–346.
14 H. Zhou, T. Yamada and N. Kimizuka, *J. Am. Chem. Soc.*, 2016, **138**, 10502–10507.
15 C. Han, X. Qian, Q. Li, B. Deng, Y. Zhu, Z. Han, W. Zhang, W. Wang, S. Feng, G. Chen and W. Liu, *Science*, 2020, **368**, 1091–1098.
16 J. T. Hupp and M. J. Weaver, *Inorg. Chem.*, 1984, **23**, 3639–3644.
17 M. A. Buckingham, K. Laws, J. T. Sengel and L. Aldous, *Green Chem.*, 2020, **22**, 6062.
18 M. A. Buckingham, K. Laws, E. Cross, A. Surman and L. Aldous, *Green Chem.*, 2021, **23**, 8901.
19 L. Aldous, J. J. Black, M. C. Elias, B. Gélinas and D. Rochefort, *Phys. Chem. Chem. Phys.*, 2017, **19**, 24255–24263.
20 L. R. Gahan and J. M. Harrowfield, *Polyhedron*, 2015, **94**, 1–51.
21 Y. Z. Voloshin, V. V. Novikov and Y. V. Nelyubina, *RSC Adv.*, 2015, **5**, 72621–72637.
22 C. Schattschneider, S. Doniz Kettenmann, S. Hinojosa, J. Heinrich and N. Kulak, *Coord. Chem. Rev.*, 2019, **385**, 191–207.
23 W. J. Maximuck and J. A. Gladysz, *Mol. Catal.*, 2019, **473**, 110360.
24 M. A. Buckingham and L. Aldous, *J. Electroanal. Chem.*, 2020, **872**, 114280.
25 M. A. Buckingham, K. Laws, H. Li, Y. Kuang and L. Aldous, *Cell Rep. Phys. Sci.*, 2021, **2**, 100510.
26 J. Zhou, Y. Che, K. Wu, J. Shen and C. He, *J. Chem. Eng. Data*, 2013, **58**, 663–670.
27 R. Ge, C. Hardacre, P. Nancarrow and D. W. Rooney, *J. Chem. Eng. Data*, 2007, **52**, 1819–1823.
28 A. Taheri, D. R. MacFarlane, C. Pozo-Gonzalo and J. M. Pringle, *Aust. J. Chem.*, 2019, **72**, 709–716.

